Energy Transfer Between Squaraine Polymer Sections: From *helix* to *zig-zag* and All the Way Back

Christoph Lambert,[a,c]* Sebastian F. Völker,[a,c] Federico Koch,[b,c] Alexander Schmiedel,[a,c] Marco Holzapfel,[a,c] Alexander Humeniuk,[b] Merle I. S. Röhr,[b] Roland Mitric,[b] and Tobias Brixner[b,c]*

a) Institut für Organische Chemie, Universität Würzburg, Am Hubland, 97074 Würzburg, Germany

b) Institut für Physikalische und Theoretische Chemie, Universität Würzburg, Am Hubland, 97074 Würzburg, Germany

c) Center for Nanosystems Chemistry (CNC), Universität Würzburg, Am Hubland, 97074 Würzburg, Germany

ABSTRACT

Joint experimental and theoretical study of the absorption spectra of squaraine polymers in solution provide evidence that two different conformations are present in solution: a *helix* and a *zig-zag* structure. This unique situation allows investigating ultrafast energy transfer processes between different structural segments within a single polymer chain in solution. The understanding of the underlying dynamics is of fundamental importance for the development of novel materials for light-harvesting and optoelectronic applications. We combine here femtosecond transient absorption spectroscopy with time-resolved 2D electronic spectroscopy showing that ultrafast energy transfer within the squaraine polymer chains proceeds from initially excited *helix* segments to *zig-zag* segments or vice versa, depending on the solvent as well as on the excitation wavenumber. These observations contrast other conjugated polymers such as MEH-PPV where much slower intrachain energy transfer was reported. The reason for the very fast energy transfer in squaraine polymers is most likely a close matching of the density of states between donor and acceptor polymer segments because of very small reorganization energy in these cyanine-like chromophores.

INTRODUCTION

Energy transfer in conjugated polymer chains is an issue of fundamental importance for the development of organic solar cells but also for many other optoelectronic devices.[1-10] Most low-molecular-weight systems possess a limited number of degrees of freedom accessible at room temperature and they often show structural flexibility that is fast even on timescales of ns. Polymers may behave totally differently compared to smaller molecules which is caused by their higher molecular weight. This brings about slower motions and, consequently, a distribution of conformers, which, because of the slower time scale, may easily influence fast electronic processes that occur in optoelectronic devices such as exciton diffusion or charge migration.[11-21] However, it is extremely difficult to gain insight into the relation of electronic processes in conjugated polymers and their microscopic or superstructure in solution and in the solid state.[22] Recently G. Scholes advanced this issue very elegantly by using MEH-PPV in its stretched form in $CHCl_3$ solution in comparison to its coiled nanoparticle form in aqueous solution.[23] These authors could show that after excitation coherence persists for some 100 fs in the stretched polymers. In the nanoparticles, interchain energy migration dominates, however. The latter is probably the more relevant scenario for condensed phases of MEH-PPV and related conjugated polymers. There it was found that interchain energy transfer is faster than intrachain energy transfer.[24] This is most likely caused by the shorter interchain distance in condensed phase and by the face-to-face orientation of localized transition moments. Some of us also determined the interplay between local morphology and energy transfer in MEH-PPV for varying temperatures around the phase-transition point using ultrafast spectroscopy[25,26].

Thus, the study of dynamic processes in polymer strands of defined structure in solution is of great importance for a better understanding of the bulk material.[27-31] However, what is lacking is information about the influence of different local structure on photoinduced processes within a single polymer strand. However, these data are decisive because conjugated polymers in solid state will usually adopt a variety of local structures that are hard to control in a deliberate way. However, in the solid state interchain processes are expected to overlay intrachain processes and both are hard to discriminate. One way of solving this dilemma is gaining such information under dilute conditions in solution phase which will exclude all interchain processes. We have recently undertaken a series of studies concerning the static and dynamic optical properties of polymeric squaraine dyes in

solution.[32-36] In this context we found a polymer whose relative amount of local superstructure (*helix* and *zig-zag*) within a single polymer strand depends on the solvent. Thus, this polysquaraine opens a unique chance to study the above mentioned intrachain processes. Both polymeric and low-molecular-weight squaraine dyes gained much attention in recent years[37] because of their typical cyanine-like behavior, that is, strong and usually narrow absorption in the red part of the visible light spectrum along with their strong fluorescence.[38-43] These properties allow many applications from dye-sensitized solar cells and organic photovoltaic applications[32,44-66] to ion sensors[67-71] and biolabelling.[72-80] Unlike conjugated polymers that are based on very small monomers such as styrene (e.g. MEH-PPV) or thiophene (e.g. P3HT) and whose polymer properties are totally different from those of the monomers,[81] squaraine homo- and copolymers are based on squaraine dyes which already show a strong absorption in the red region of the visible spectrum.[32-36] The optical properties of the squaraine polymer, although distinct from those of the monomeric dye, can be explained by exciton coupling of localized squaraine chromophore transition moments which in general leads to broadened and red-shifted spectra reflecting the excitonic manifold of states. Accordingly, the red-shifts into the NIR spectral region and changes of absorption band shapes were discussed.

For the squaraine homopolymer $[SQB]_n$ (see Figure 1) we found evidence that the superstructure in solution depends on the solvent.[36] Thus, in some solvents (e.g. DCM, $CHCl_3$) stretched polymer chains dominate which leads to a pronounced red-shifted absorption (J-aggregate behavior = head-to-tail arrangement of transition moments) compared to the monomer absorption, while in others (e.g. acetone), the polymers mostly adopt a helix conformation which displays a blue-shifted most intense absorption (H-aggregate behavior = face-to-face arrangement of transition moments) of the exciton manifold.[33] In DMF, obviously mixtures of both superstructures are present within one polymer strand. The assignment to specific structural motifs was derived from a variety of computed (semiempirical AM1 method) structural models whose computed absorption spectra (INDO method) agree with the measured spectra when e.g. the spectra of *helix* and of *zig-zag* structures with different ratios are superimposed. While this picture is certainly highly simplistic, it is able to explain the basic spectral features very well. Further support on this structural assignment with the help of computed absorption spectra will be given below based on more elaborate DFT calculations.

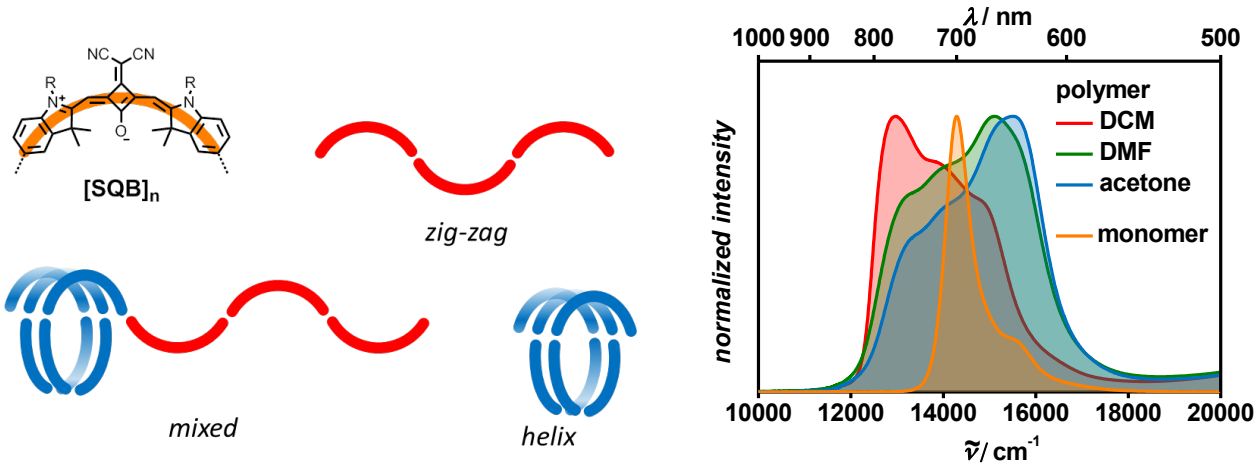

Figure 1. Proposed polymer structures of $[SQB]_n$ and absorption spectra in diverse solvents.

In this work, we will assess the photoinduced dynamics of the $[SQB]_n$ polymer in two different solutions, in DCM where predominantly stretched polymer chains prevail, and in DMF where, besides stretched sections, the polymer possesses mainly helix sections. By transient absorption pump-probe spectroscopy[82] we will show that the dynamics are significantly different in these two solvents which can be traced back to the different superstructure. Finally, support for the interpretation is given by coherent two-dimensional (2D) electronic spectroscopy, as it separates signal contributions into excitation and detection energies[83-86]. With 2D spectroscopy we monitor the energy relaxation of excited chromophores within different structural domains.

EXPERIMENTAL

Spectroscopic methods

For all spectroscopic experiments squaraine homopolymer $[SQB]_n$ with $M_w = 46700$, PDI = 1.8, and $X_n = 36$ was diluted in DMF or DCM to achieve an optical density OD ≈ 0.3 at the respective excitation wavenumber.

Transient absorption spectra of the squaraine polymer were obtained by pumping $[SQB]_n$ with ca. 140 fs laser pulses (1 kHz) generated by an amplified Ti-sapphire oscillator (fundamental 800 nm = 12500 cm^{-1}) and an OPA for generating the appropriate excitation wavenumber (13200 cm^{-1} and 15200 cm^{-1}) and probed with a white-light continuum generated with a small portion of the

fundamental focused in a CaF_2 crystal. Transient absorption data were analyzed with the global and target analysis program GLOTARAN based on the statistical fitting package TIMP.[87-89] The results of a parallel fitting model are presented in the wavelength domain as decay-associated difference spectra (DADS).[90] Every DADS corresponds to the wavelength-dependent amplitudes of one exponential decay component. Furthermore, results of a target model are presented with species-associated difference spectra (SADS) each of which belongs to one species that may be populated or depopulated by several paths.

Coherent optical 2D experiments were performed in an inherently phase-stable 2D setup, described extensively elsewhere.[91] Briefly, excitation pulses centered at 13700 cm^{-1} (730 nm) were realized by using a commercial noncollinear optical parametric amplifier (NOPA, TOPAS-white, Light Conversion Ltd.) pumped by a commercial Ti:sapphire regenerative-amplifier laser system (Spitfire Pro, Spectra Physics) with output pulses centered at 800 nm with 120 fs duration and 1 kHz repetition rate. Pulse durations at the sample position were 22 fs for the experiments in DCM and DMF as determined from SHG-FROG in a 10-μm β-barium borate (BBO) crystal. For each population time T (time delay between pulses 2 and 3), the coherence time τ (time delay between pulses 1 and 2) was varied between $\tau = \pm 120.69$ fs in steps of $\Delta\tau = 4.47$ fs. Real-valued 2D spectra, reflecting the change in absorption, were obtained by phasing with transient absorption data within the same experimental setup using beam 3 as a probe. Optical signals were spectrally dispersed and detected via a spectrograph (Acton SP2500i) equipped with a CCD camera (Princeton Instruments Pixis 2k).

Computational methods

The optical spectra of the extended (*zig-zag*) and *helix* form of the model SQB hexamer were calculated using the recently introduced long-range-corrected tight-binding time-dependent density functional theory (lc-TDDFTB)[92]. Since the details of the lc-TDDFTB method have been published elsewhere[92], we only provide a brief summary here. The lc-TDDFTB method has been introduced as an approximate and highly efficient alternative to the long-range-corrected TDDFT,[93] which is applicable to much larger systems containing up to several thousands of atoms. This method introduces the long-range correction to the linear response version of the time-dependent density functional tight binding method (TDDFTB)[94] by adding an exact Hartree-Fock exchange term, which is switched on at large distances, to the ground-state DFTB Hamiltonian[95] as well as to the TDDFTB coupling matrix. We wish to emphasize that the inclusion of the long-range correction is mandatory in

order to exclude the contamination of the spectra by spuriously low charge-transfer states, which typically occur in conventional TDDFT and TDDFTB and might pose a serious problem, in particular in multichromophoric oligomers and polymers.

Based on the geometries obtained from the semiempirical AM1 calculations[36] the ground-state electronic structure has been first calculated using the self-charge-consistent DFTB with the long-range correction included into the ground-state Kohn-Sham (KS) Hamiltonian. This provides occupied and virtual KS orbitals, which are subsequently used to calculate the optical spectra. The latter are obtained by solving the linear response equation in the Tamm-Dancoff approximation (TDA). As we have shown recently, the TDA approximation in connection with the long-range correction actually leads to better excitation energies in comparison with the full solution of the linear response equations, in particular in cases in which singlet-triplet instabilities would lead to imaginary excitation energies. The solution of the linear response problem provides the excitation energies and excitation coefficients which were used to calculate the transition dipole moments and oscillator strengths of the optical transitions. For this purpose we employ Slater-Koster tables for the dipole matrix elements between valence orbitals, which provides a more accurate description of the oscillator strengths than the commonly used Mulliken transition charge approximation. The character of the excited states has been analyzed by computing the electronic transition densities. The expected accuracy of the lc-TDDFTB approach is comparable to the full long-range-corrected TDDFT (CAM-B3LYP). Our tests on a large suite of molecules gave rise to an average error of the transition energies for excited states with local or delocalized character between 0.3-0.4 eV. While not fully quantitative, this allows us to reproduce the overall shape of the experimental spectra reasonably well and to provide the assignment of the spectral features to the structural motifs.

RESULTS AND DISCUSSION

Computations

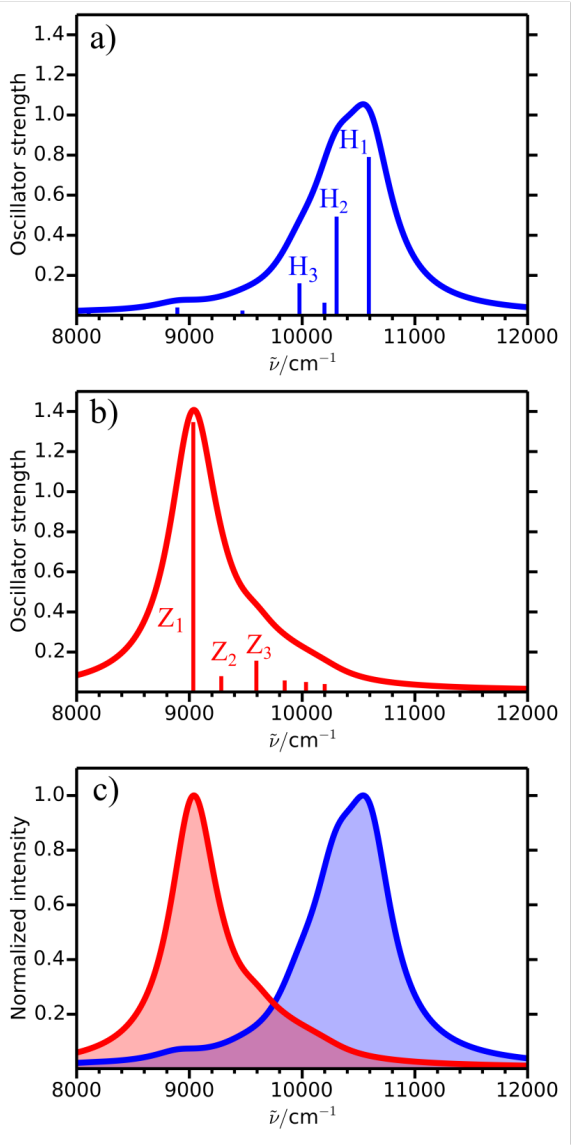

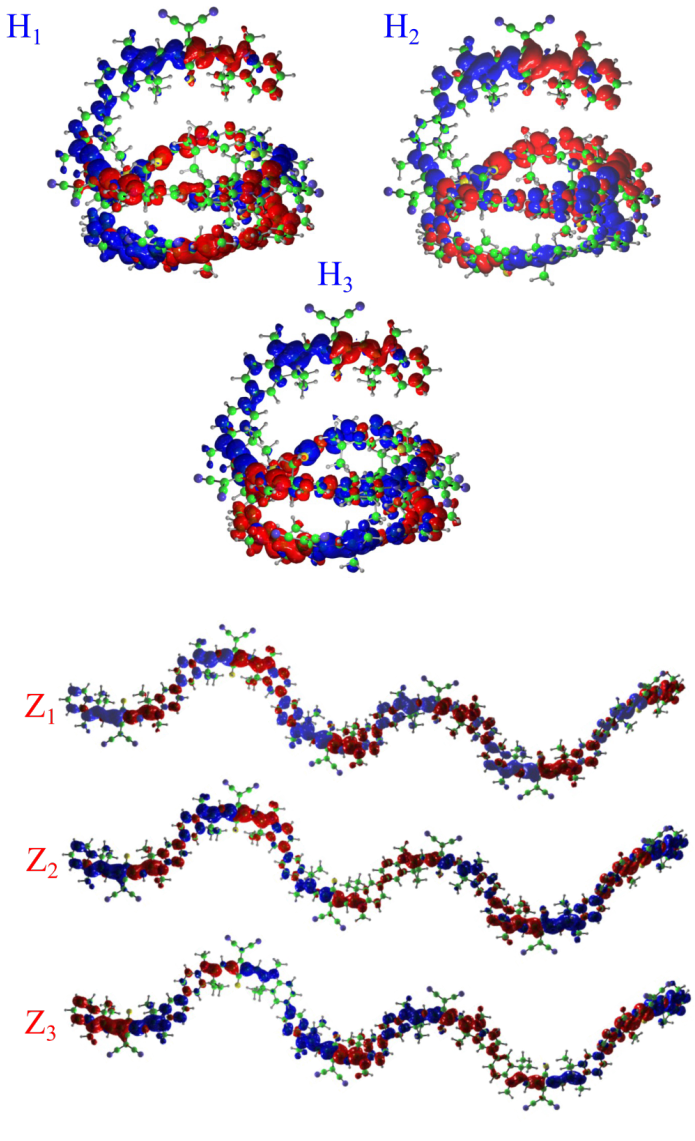

Figure 2. Calculated absorption spectra of the a) *helix* and b) extended (*zig-zag*) conformers of a model SQB hexamer. The labels $H_{1\text{-}3}$ and $Z_{1\text{-}3}$ denote the three most intense transitions for the *helix* and *zig-zag* conformer, respectively. c) Comparison of the theoretical normalized absorption spectra for both conformers. d) The transition densities for the three most intense transitions of both conformers are presented on the right hand side of the figure.

The strongest absorption band of the *helix* conformer is located at 10600 cm^{-1} and is accompanied by two weaker bands at 10300 and 9980 cm^{-1} (Figure 2a). These three bands belong to the first exciton manifold, which arises due to the electronic coupling between the first excited states of six individual monomeric units. The excitonic character is illustrated by the calculated transition densities shown in Figure 2d (H_1-H_3). The transition densities for all three states are strongly delocalized along the *helix* structures and differ by the signature (phase) on the individual monomeric units. Since in the *helix* structure, the individual chromophores are stacked, a H-type (face-to-face) coupling occurs leading to the highest intensity of the most blue-shifted intense band H_1. We also note that the first excitonic manifold consists of six transitions with a "band" splitting of ca. 1750 cm^{-1} (cf. Figure 2a).

In contrast, the absorption spectrum of the extended *zig-zag* conformer exhibits a most intense transition which is strongly red-shifted with respect to the most intense transition of the *helix* structure and is located at 9000 cm^{-1}. The intense band is accompanied by two weaker peaks at 9280 and 9600 cm^{-1} (Figure 2b). The transition densities for the three lowest-lying intense bands are presented in Figure 2d (Z_1-Z_3). Again, the transition densities are fully delocalized over the extended structure and reflect the coupling of transition dipole moments on individual monomers. For example, in the most intense transition Z_1 all monomers are coupled in a head-to-tail manner with transition dipoles pointing in the same direction, which is a characteristic J-aggregate behaviour. The total splitting of the first excitonic band is ca. 1200 cm^{-1}, lower than for the *helix* structure. The smaller bandwidth of the *zig-zag* structure is in agreement with the experimental findings.

In order to emphasize the spectral differences between the *helix* and the extended conformation we also present the theoretical normalized spectra of both species in Figure 2c. It can be clearly seen that the spectrum of the extended structure is strongly red-shifted with respect to the one for the *helix* structure. The theoretical spectra can be compared with the experimental spectra of the SQB polymers presented in Figure 1. Since we expect that the spectral features of the model hexamer system are of general nature and will also be characteristic for the spectral properties of longer oligomers and polymers, we assign the spectrum in DCM to the *zig-zag* type of structure. In acetone or DMF the theoretical calculations support the assignment to the *helix* structure.

Transient absorption

In DCM where the $[SQB]_n$ polymer adopts mainly the elongated *zig-zag* structure we performed two different pump-probe experiments: in the first experiment (hereafter called experiment 1), we pumped the sample at 13200 cm^{-1} where the *zig-zag* structure shows the highest extinction coefficient and, thus, will be predominantly excited. Accordingly, right after the excitation the transient spectra (Figure 2a) show a strong ground-state bleaching (GSB) at ca. 13000 cm^{-1}, which experiences a little red-shift within the first ps. Much weaker GSBs are seen at ca. 15000 cm^{-1} and at ca. 25000-26000 cm^{-1}. There is also a broad but weak excited-state absorption (ESA) between 16000-24000 cm^{-1}. All these signals decay with only little changes of their relative intensities. In Figure 2, the time traces directly reflect the population of excited *zig-zag* segments (time trace at 12900 cm^{-1}) and excited *helix* structure (time trace at 15200 cm^{-1}). These findings support that almost exclusively *zig-zag* chains have been excited which relax to the ground state.

a) *Experiment 1*

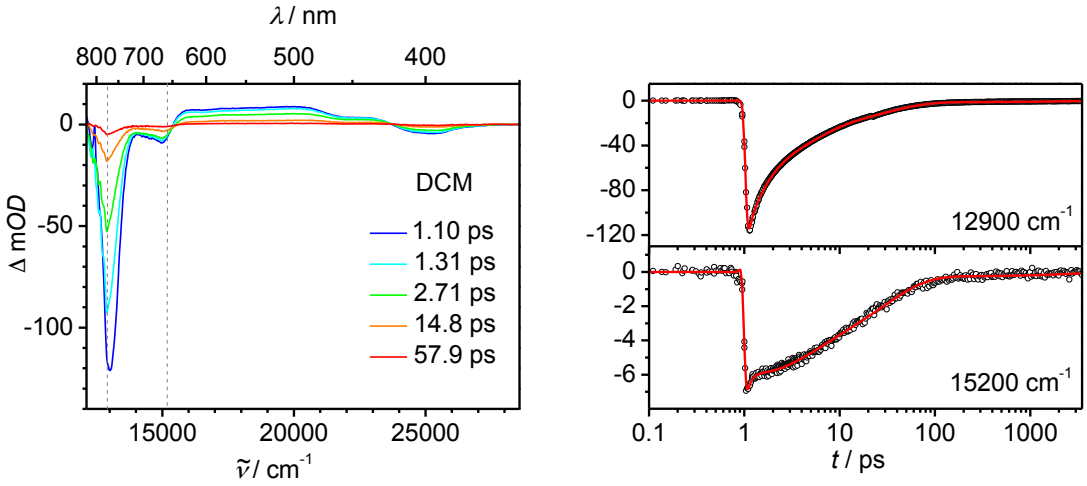

b) *Experiment 2*

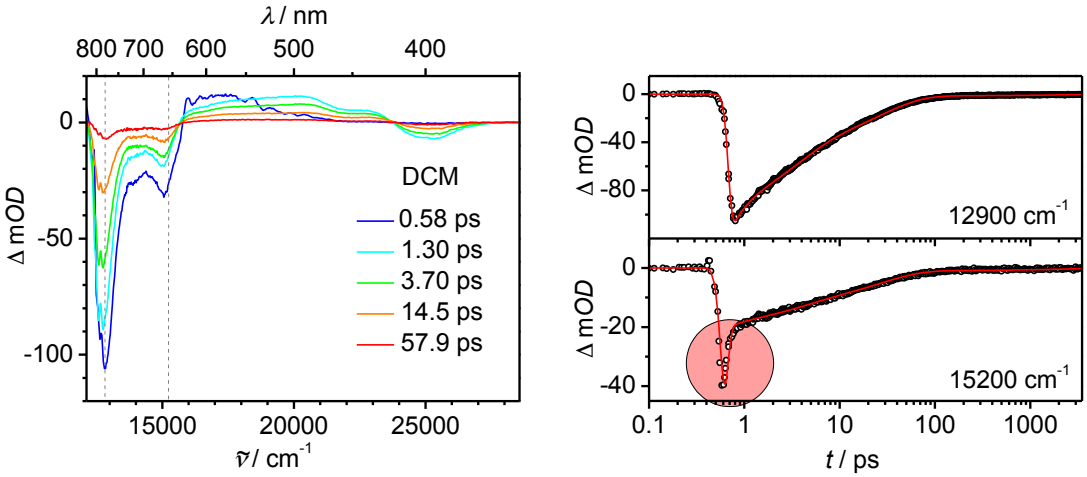

Figure 2. Selected transient absorption spectra (stray light and chirp corrected; early spectra are given in blue, later spectra in red) and selected time traces with global fit (red lines) of $[SQB]_n$ in DCM at a) 13200 cm^{-1} pump wavenumber and b) at 15200 cm^{-1} pump wavenumber. The wavenumbers of the time traces are given by grey dashed lines in the spectra diagrams.

In the second experiment (= experiment 2), we pumped the same sample at 15200 cm^{-1} which excites those few polymer sections which possess a *helix* structure. While the transient spectra (Figure 2b) are generally similar to those of the first experiment (13200 cm^{-1} excitation), a closer inspection shows some delicate differences: again, the strongest GSB is at 13000 cm^{-1} but there is now also a pronounced GSB at 15000 cm^{-1}. The former indicates excitation of *zig-zag*, the latter of *helix* structures. However, the 15000 cm^{-1} GSB decays more rapidly within the first ps than that at 13000 cm^{-1}. This rapid decay can be seen in the corresponding time traces in Figure 2b (at 15200 cm^{-1}, marked with a red circle). From then on the transient spectra look very similar to those of experiment 1. Thus, in both experiments after ca. 1 ps we end up with excited *zig-zag* polymer strands, which indicates that energy transfer from the helix segments to the *zig-zag* segments within one polymer strand must have occurred. At this point, we stress that the sample solutions are very diluted which excludes energy transfer between different polymer strands.

a) *Experiment 3*

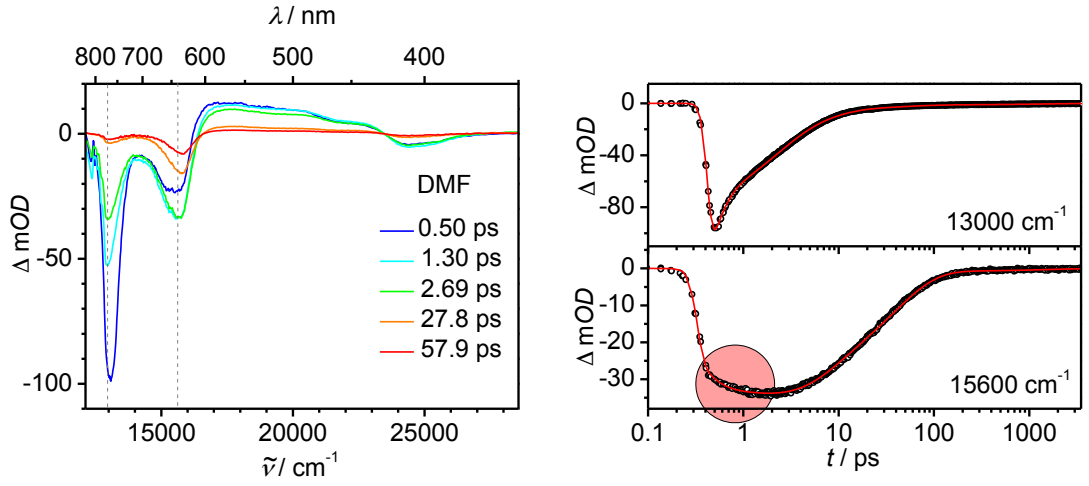

b) *Experiment 4*

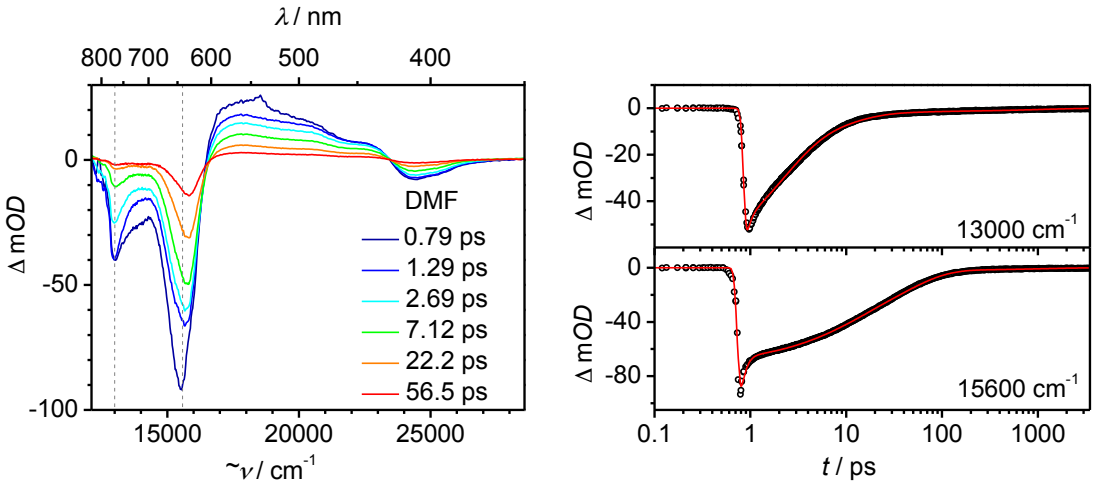

Figure 3. Selected transient absorption spectra (stray light and chirp corrected; early spectra are given in blue, later spectra in red) and selected time traces with global fit (red lines) of $[SQB]_n$ in DMF at a) 13200 cm^{-1} pump wavenumber and b) at 15200 cm^{-1} pump wavenumber. The wavenumbers of the time traces are given by grey dashed lines in the spectra diagrams.

In order to elucidate the impact of structure on the photoinduced dynamics we also performed two pump-probe experiments of the $[SQB]_n$ polymer in DMF solution. Here, the polymer strands possess predominantly a helix conformation. Excitation at 13200 cm^{-1} (= experiment 3) yields transient spectra (see Figure 3a) with a strong GSB at ca. 13000 cm^{-1} together with ESA and GSB signatures at lower wavenumber similar to the DCM experiments. The strong GSB again shows a little red-shift

and decays to ca. 2/3 of the initial intensity within the first ps. At the same time another GSB at ca. 15000 cm^{-1} grows in, as can easily be seen in the time traces at 15600 cm^{-1} (marked with a red circle in Figure 3a). This leads to a reversal of relative GSB intensities at 13000 cm^{-1} and 15000 cm^{-1} within the first 10 ps. After 20 ps the GSB at 13000 cm^{-1} has almost disappeared. The transient spectra at $t > 20$ ps thus indicate almost exclusive population of excited *helix* structures. In contrast to the results in DCM, the observations made in DMF indicate energy transfer from *zig-zag* to *helix* segments within one polymer strand. In the second pump-probe experiment in DMF (= experiment 4), the sample was pumped at 15200 cm^{-1}, thus exciting *helix* segments. Initially, the transient spectra show both a very intense GSB at ca. 15600 cm^{-1} but also a prominent GSB at ca. 13000 cm^{-1}. The former decays rapidly within the first ca. 100 fs (time trace at 15600 cm^{-1}, Figure 3b) and from then on more slowly. The GSB at ca. 13000 cm^{-1} behaves differently. It does not show the very rapid decay at the beginning but decays overall much faster at later times than the 15600 cm^{-1} GSB. In the end, the transient spectra are left with a strong GSB at ca. 15600 cm^{-1} again indicating almost exclusive excited-state population of *helix* structures.

Global Analysis. Taken together, the above sketched experiments indicate energy transfer processes from *helix* to *zig-zag* segments (experiment 2) and from *zig-zag* to *helix* structures (experiment 3). This can only be understood if the lowest excited state has *zig-zag* structure in DCM but *helix* structure in DMF. In order to assess the number of spectral components to the transient spectra we performed a global analysis of the transient map (absorbance change as a function of wavenumber and time) using the GLOTARAN software. This analysis gave five components in all cases as depicted in Figure Sx in Supplementary Information (SI) in form of decay-associated difference spectra (DADS, parallel decay mechanism). However, the fifth component has a very small amplitude in all cases and was therefore disregarded in further discussions which can be found in the SI.

Target Analysis. The above presented data (Figures 2 and 3 and the DADS in SI) and evaluated information were used to develop a kinetic model both for the experiments in DCM and in DMF to which the transient data were globally fitted (target analysis). In these target models we assumed an energy transfer from *helix* to *zig-zag* segments (see experiment 2) and an energy transfer from *zig-zag* to *helix* segments (see experiment 3) and both processes for experiment 4. Furthermore, we assumed that the extinction coefficients of all species at ca. 18800 cm^{-1} is equal for all transient species as ESA to higher lying states should have the same extinction coefficient. This requires to introduce additional pathways connecting the transient species and to adjust the efficiencies for each particular

pathway. The outcome of these target analyses are species-associated difference spectra (SADS) which are given together with the kinetic pathways in Figure 4 for DCM and in Figure 5 for DMF.

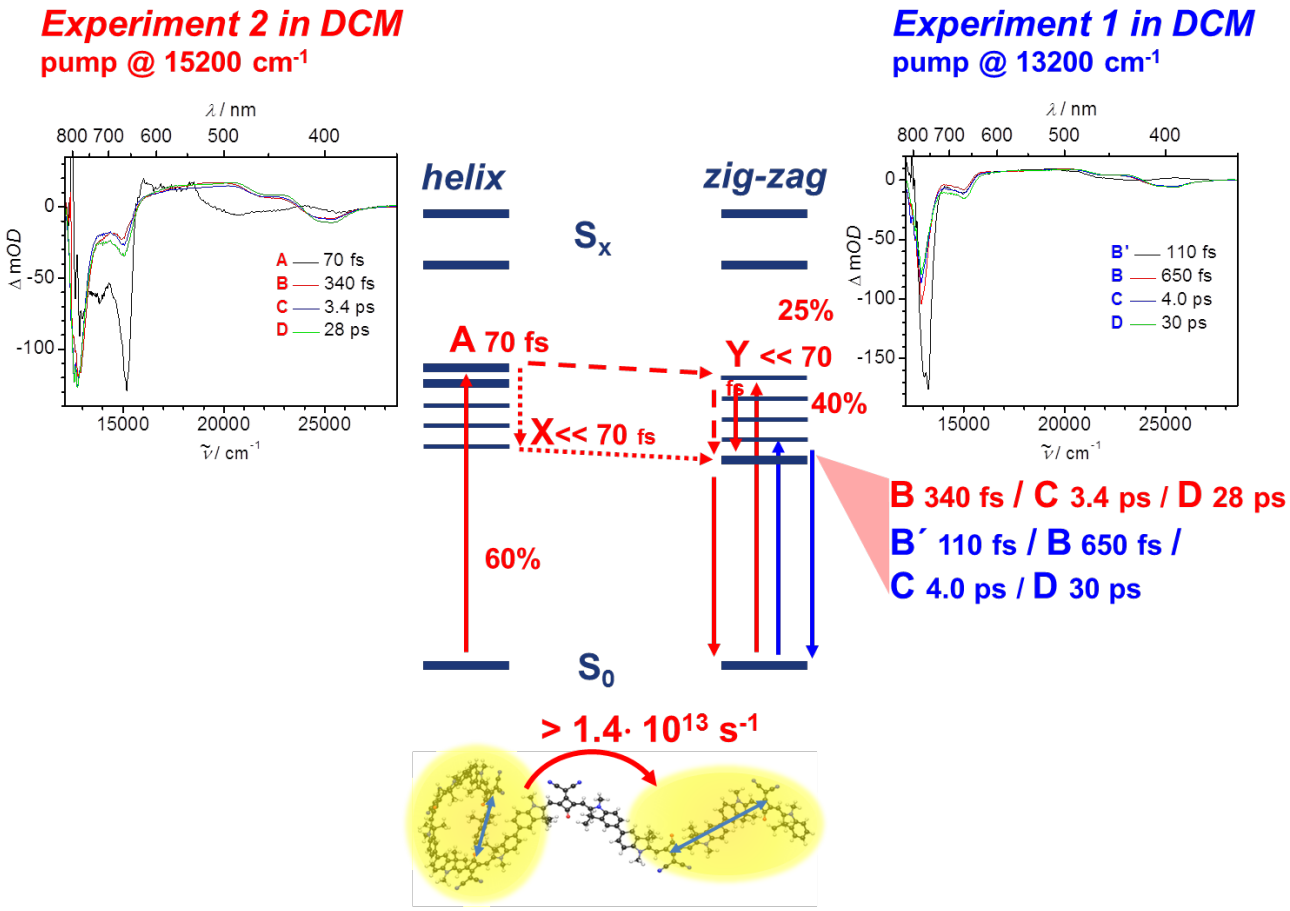

Figure 4. Species-associated difference spectra of $[SQB]_n$ in DCM at 15200 cm^{-1} (left) and 13200 cm^{-1} (right) pump energy. State diagrams (the number of exciton states is arbitrary) of *helix* and *zig-zag* sections (middle). Assignments and data given in red pertain to experiment 2, those given in blue to experiment 1.

For experiment 2, the target analysis in Figure 4 indicates a parallel excitation of *helix* and *zig-zag* structure in a 60:40 ratio. These states are labelled "A" and "Y" in Figure 4. The SADS of A shows prominent bleaching signals at 15200 cm^{-1} (black spectrum in the left inset in Figure 4). Species Y relaxes in an ultrafast process to B and is therefore not visible in the spectra. Species A has a lifetime of 70 fs. This could either mean that it relaxes first within the exciton manifold to X from which ultrafast (τ << 70 fs) energy transfer to B occurs (in that case X is also not visible in the spectra because of its low intermediate concentration) or that A first undergoes energy transfer with τ = 70 fs

to Y and then relaxes in an ultrafast process. We cannot discriminate between both cases (given by dashed and dotted lines in Figure 4) by kinetic methods but can give an upper bound for the rate of energy transfer from *helix* to *zig-zag* structure with 1/(70 fs) ($k_{A\rightarrow B}$ = 1.4·10^{13} s^{-1}). However, we will give below evidence that the latter mechanism (dashed lines) is at work (see experiment 4). In either case, the relaxation process within the exciton manifold from A into B can be followed by the spectral changes of the ESA around 18200-25000 cm^{-1}. The SADS of B-D are quite similar to each other with a prominent bleaching at ca. 13000 cm^{-1} which indicates excited *zig-zag* population. From B, two structural relaxation processes lead via C and D with τ = 340 fs and τ = 3.4 ps by depopulation with τ = 28 ps into the ground state. The efficiencies for the latter processes can be found in Table S1 in the SI.

Direct excitation of the *zig-zag* structures of the squaraine polymer in DCM at 13200 cm^{-1} in experiment 1 is followed by relaxation within the exciton manifold from B' to B with τ = 110 fs. This process goes along with spectral changes of the ESA between 20000-25000 cm^{-1} (see right inset in Figure 4). From then on, structural and excited state depopulation processes occur very similarly to the ones in experiment 2 concerning their DADS and the associated lifetimes.

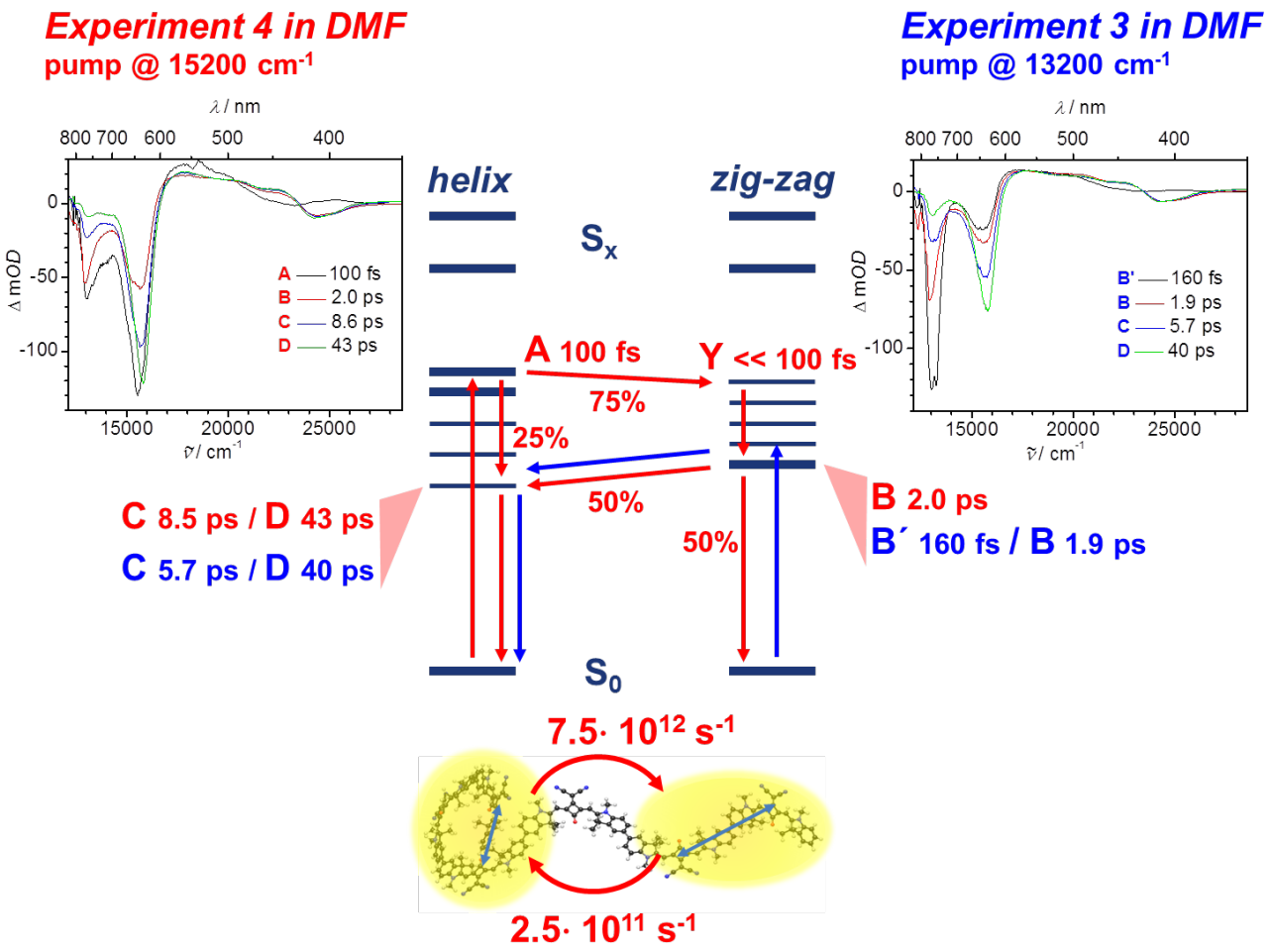

Figure 5. Species-associated difference spectra of $[SQB]_n$ in DMF at 15200 cm^{-1} (left) and 13200 cm^{-1} (right) pump energy. State diagrams (the number of exciton states is arbitrary) of *helix* and *zig-zag* sections (middle). Assignments and data given in red pertain to experiment 4, those given in blue to experiment 3.

In DMF excitation of the *zig-zag* segments at 13200 cm^{-1} (experiment 3) yields first an SADS with a very strong GSB at ca. 13000 cm^{-1} (black spectrum of B' in the right inset in Figure 5) and subsequent SADS (spectra of B-D in the right inset in Figure 5) with decreasing GSB at this wavenumber but increasing GSB at ca. 16000 cm^{-1} (see right inset in Figure 5). Unlike experiment 1 and 2 in DCM where the SADS of species B-D were spectrally very similar, in DMF the relative intensity of the GSB at 13000 cm^{-1} and at 16000 cm^{-1} change stepwise on going from B' to D. We assume that this is caused by a broader distribution of *helix* and *zig-zag* segments within a polymer strand. Nevertheless, the sequence of SADS indicates energy transfer from excited *zig-zag* states to excited *helix* states which we assign to the $\tau = 1.9$ ps step where the strongest changes in intensity at

13000 cm^{-1} and at 16000 cm^{-1} are apparent. Again, the spectral difference between the SADS of B' and of B around 21000-27000 cm^{-1} are associated with changes in ESA upon relaxation within the exciton manifold. This is due to the fact that we excited the sample at the maximum of the lowest energy band which still is somewhat higher in energy than the lowest exciton state.

In experiment 4 where the *helix* segments are primarily excited, we observed a series of SADS with decreasing GSB at ca. 15000 cm^{-1}. At 13000 cm^{-1} the situation is more complicated inasmuch as the GSB displays only little decrease between the first (black spectrum of A in the left inset in Figure 5) and the second SADS (red spectrum of B in the left inset in Figure 5) but then a rapid decrease until an SADS reflecting purely excited *helix* states has developed (green spectrum of D in the left inset of Figure 5). In analogy of experiment 2 we interpret these findings with an energy transfer from excited *helix* segments to excited *zig-zag* segments with τ = 100 fs. From the efficiency of this pathway (75%) we evaluate a rate constant of $k_{A\rightarrow B} = 7.5\cdot10^{12}$ s^{-1} for this energy transfer process which in turn is followed by ultrafast relaxation within the exciton manifold of the *zig-zag* segments to give species B. This excited species has a lifetime of τ = 2.0 ps (very similar to experiment 3 with τ = 1.9 ps) and undergoes back-energy transfer (*zig-zag* to *helix* segments) to C with $k_{B\rightarrow C} = 2.5\cdot10^{12}$ s^{-1} and an efficiency of 50%. Subsequent relaxation of C into D and depopulation of D into the ground state occurs with τ = 8.5 and 43 ps. At this point we stress that equally good target fits could be obtained by assuming a parallel excitation of *helix* and *zig-zag* sections followed by energy transfer from excited *zig-zag* to *helix* segments. While we cannot fully rule out this scenario, it appears to be unlikely based on the analysis of experiment 2, where the energy transfer *helix* ⟶ *zig-zag* is obvious. This energy transfer, for which we obtained an efficiency of 75% in experiment 4, requires that the relaxation within the exciton manifold of the *helix* segments is much slower ($k_{A\rightarrow C} = 2.5\cdot10^{12}$ s^{-1}) than the energy transfer step. Adopting this interpretation also rules out the dotted pathway in experiment 2 (Figure 4) in DCM (see above).

The above outlined analysis results in three major points: First, in DCM the lowest exciton state of *zig-zag* segments is lower in energy than the lowest exciton states of *helix* segments. In DMF the situation is vice versa. Second, relaxation within the exciton manifold of the *helix* segments is much slower than in the *zig-zag* segments. And third, energy transfer from the *helix* segments to the *zig-zag* structures is an order of magnitude faster than from *zig-zag* to *helix* segments.

Concerning point 1: The exciton coupling in a *helix* structure and, consequently the exciton bandwidth might be larger than in a *zig-zag* structure because the individual squaraine chromophores can be closer in the face-to-face arrangement of a helix. The difference of interchromophore distances is sketched in the molecular structure in Figure 4 by blue arrows. Therefore, the electronic structure depends strongly on the supramolecular structure and a somewhat smaller bandwidth with a higher-lying lowest energy exciton state is expected for e.g. looser helix arrangements in DCM than in DMF. The relaxation within the exciton manifold and the energy transfer processes (point 2 and 3) both depend on Franck-Condon overlap of states. In general the relaxation within an exciton manifold depends strongly on exciton-vibrational coupling and may also lead to "transient population trapping"[96] in vibrationally excited states. These effects, though hardly predictable in complex systems such as $[SQB]_n$ may influence the relative relaxation rates *within* the exciton manifold vs. *between* the different polymer sections.

2D Spectroscopy

To visualize the initial interactions and relaxation dynamics between the absorption bands of the polymer we performed coherent 2D spectroscopy using a laser spectrum covering the absorption maxima at ≈ 13000 cm^{-1} and ≈ 14000 cm^{-1}. Figure 6 depicts the results for $[SQB]_n$ in DCM (a) and DMF (d) for selected population times *T*. Excitation corresponds to the horizontal $\tilde{\upsilon}_\tau$ wavenumbers, and detection corresponds to the vertical $\tilde{\upsilon}_t$ wavenumbers. Blue (positive) signals display GSB and SE signal contributions, while red (negative) signals display ESA contributions. As a consequence of the limited laser pulse bandwidth (Fig. 6b for $[SQB]_n$ in DCM and Fig. 6e for $[SQB]_n$ in DMF), covering ≈ 1500 cm^{-1} of the spectrally broad absorption band, the dynamics within these bands are visible as 2D line-shape modifications rather than clearly separated peaks. For the population time $T = 0$ fs, signal contributions of the solvent have to be taken into account. Furthermore, "phase twist" contributions originating from the temporal overlap of the third pulse with the first two may occur.

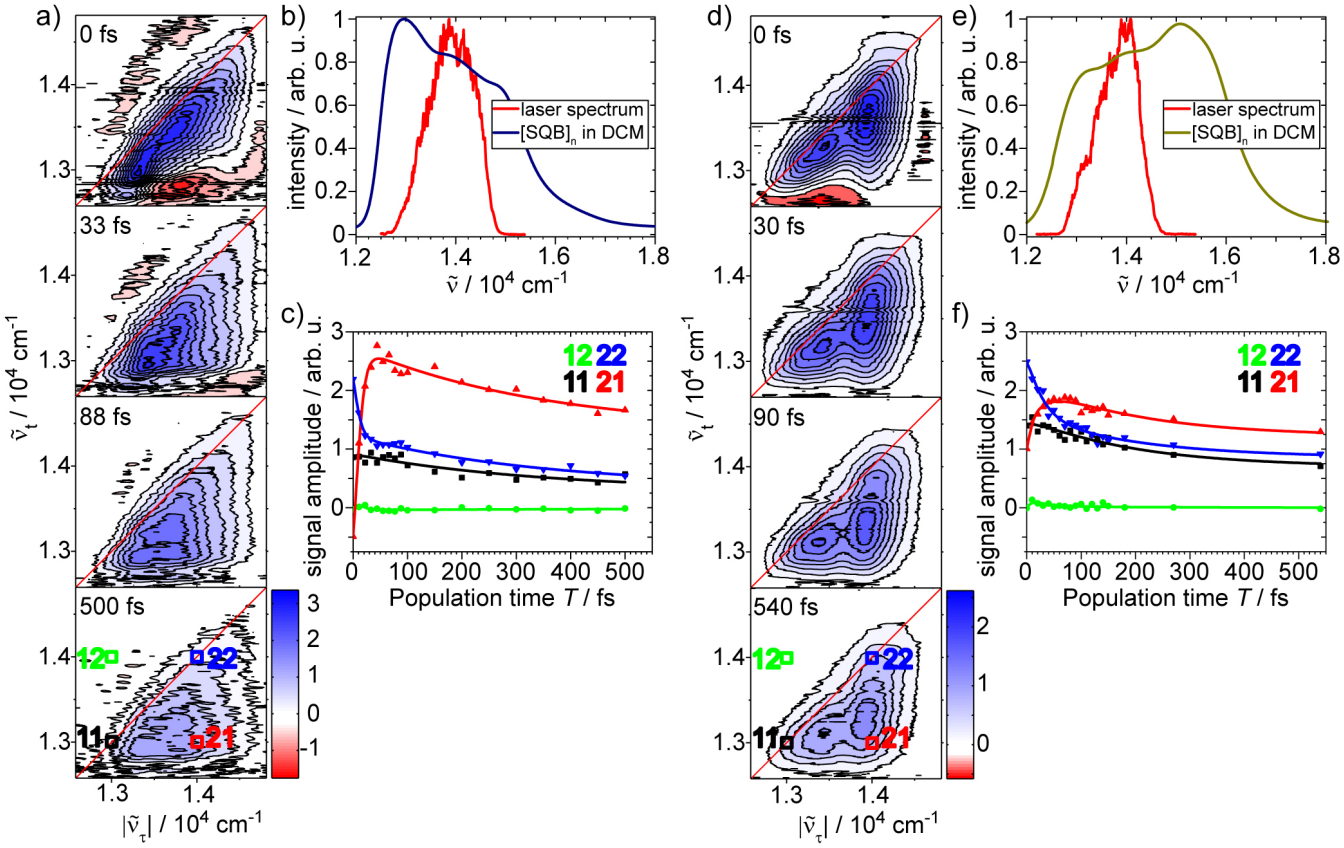

Figure 6. Coherent 2D spectroscopy of $[SQB]_n$ in DCM (a) and DMF (d) for selected population times. 2D spectra have been normalized to the maximum value of the $T = 0$ fs spectrum and contour lines are drawn in steps of 10% starting at from 95%. b) and e) display the laser and absorption spectrum during the 2D scan in DCM (b) and DMF (e). c) and f) depict the dynamics of the diagonal and off-diagonal signal amplitudes for four ROIs of $[SQB]_n$ in DCM (c) and DMF (f) marked in the lowest 2D spectrum.

The laser pulses centered at 13700 cm^{-1} mainly excite intermediate sections of the polymer which are energetically between the absorption of *zig-zag* and *helix* segments. Qualitative similarities can be found in the real-valued 2D spectra of $[SQB]_n$ in DCM and DMF: The $T = 0$ fs spectrum is mainly elongated along the diagonal for horizontal $|\tilde{\nu}_\tau| \lesssim 13750$ cm^{-1}, i.e. excitation and emission frequencies are correlated. For higher excitation wavenumbers already a coupling to lower detection wavenumbers is observable as a larger shift of the signal below the diagonal. The subsequent dynamics within the first 90 fs are governed by an ultrafast component that is associated with changes in the 2D lineshape: At high excitation wavenumbers the signal loses its amplitude and gains intensity at lower detection wavenumbers. Between 90 fs and 500 fs an overall decay of the signal can be observed.

In order to get a better impression of the signal amplitude progression in the 2D spectra, we chose four square regions of interest (ROI) with a side length of ≈ 115 cm^{-1} centered at the diagonal ($\tilde{\upsilon}_\tau = \tilde{\upsilon}_t$) and off-diagonal ($\tilde{\upsilon}_\tau \neq \tilde{\upsilon}_t$) positions corresponding to absorption maxima at ≈ 13000 cm^{-1} and ≈ 14000 cm^{-1}. The signal evolution of these ROIs is shown in Fig. 6c for $[SQB]_n$ in DCM and Fig. 6f for $[SQB]_n$ in DMF as a function of population time (symbols). Starting at $T = 0$ fs, the diagonal peaks (11 and 22) have the highest amplitude. With increasing T the strongest changes are the initial decrease of the 22 accompanied by the rise of the corresponding off-diagonal peak 21. After this process the overall amplitude of all components decreases up to our measurement limit of $T \approx 500$ fs.

To quantify these processes we performed, for each solvent, global fits of the four ROI signal over time, i.e. sharing the rates while amplitudes and offset were free parameters. For $[SQB]_n$ in DCM the fit resulted in two time constants of $1/k = 9\pm2$ fs and 349±118 fs, and in DMF the time constants were $1/k = 28\pm7$ fs and 201±53 fs. In both solvents we observe ultrafast energy transfer from initially excited states towards energetically lower-lying states on the order of our pulse duration. According to the global fit the cross-peak 21 rises with the same time constant as a decay of the corresponding diagonal peak 22. This indicates an ultrafast relaxation within the excitonic manifold towards the lowest states in energy as was assumed in the global target fit in Figures 4 and 5. From the latter states further relaxation processes occur which lead to an overall decay of the signal without a change in line-shape within our spectral and population time window. The subsequent relaxation displays the relaxation of the *zig-zag* segments in DCM with 1/k = 349 fs and in DMF with $1/k = 201$ fs. The time of 349 fs (from the 2D analysis) fits well with the lifetime of B observed in the transient absorption experiment 2, whereas the time of 201 fs in DMF (from the 2D analysis) fits well with the lifetime of B' in the transient absorption experiment 3.

In the 2D spectroscopy experiments we excited mainly energetically intermediate states of the polymer. In DCM an ultrafast relaxation towards the lowest *zig-zag* energy takes place, followed by a further relaxation of this state. In DMF the coupling between intermediate states and *zig-zag* states is already visible in the $T = 0$ fs 2D spectrum as a pronounced off-diagonal signal. Subsequently, the energy relaxes towards the *zig-zag* states within $1/k = 28$ fs from where further relaxation towards the energetically more stable *helix* (in DMF) may occur with $1/k = 201$ fs. We interpret this as an energy-driven process: in DCM there are mainly *zig-zag* segments which are the lowest in energy. The excited intermediate states relax initially towards these *zig-zag* states in DCM, while in DMF the

relaxation from the excited intermediate states towards the *helix* segments is coupled via the *zig-zag* conformations.

CONCLUSIONS

The DFT computations have confirmed that the *zig-zag* polymer strands behave like J-aggregates and the *helix* segments like H-aggregates concerning their optically allowed transitions. Based on these structural models which are to a different degree present in DCM and DMF solutions of $[SQB]_n$ we analyzed the transient absorption measurements and fitted the results to target models which give a consistent picture of all relaxation processes within the exciton manifolds and between the different *helix* and *zig-zag* segments within single polymer strands. In addition, the relaxation processes on the sub-picosecond timescale were confirmed by 2D spectroscopy. Taken this information together we could show that excitation of *helix* segments in DCM at higher pump wavenumber is followed by energy transfer to the *zig-zag* sections ($k \sim 10^{13}$ s^{-1}). In DMF the situation is somewhat more complex, excitation of the *zig-zag* sections at lower pump wavenumber results in energy transfer to *helix* sections but direct excitation of the *helix* sections at higher wavenumber initiates first an energy transfer to the *zig-zag* segments ($k \sim 10^{13}$ s^{-1}), followed by an energy back-transfer to the *helix* sections ($k \sim 10^{11}$ s^{-1}). This shows that energy transfer between different structural sections within one polymer chain is faster than relaxation within the exciton manifold in the present case and supports an assumption made quite recently[33] that energy transfer within polymer chains of squaraines may be well below the sub-picosecond time scale. These observations contrast other conjugated polymers such as MEH-PPV where much slower intrachain energy transfer was found.[3,24] The reason for the very fast energy transfer in squaraine polymers is most likely a matching of the density of states between donor and acceptor states because of very small reorganization energy in this class of cyanine-like chromophores.[33] In the more conventional-type polymers polyphenylenevinylene and polythiophene this energy-state matching is obviously weaker as can be seen by a strong Stokes shift and the small spectral overlap of absorption and fluorescence spectra.[97] Thus, if ultrafast energy transfer is wanted, the use of polymers based on cyanine-like chromophores such as squaraines may be advantageous.

ASSOCIATED CONTENT

Transient absorption spectra and global analysis data. This material is available free of charge via the Internet at http://pubs.acs.org.

AUTHOR INFORMATION

Corresponding Authors

*(C.L.) christoph.lambert@uni-wuerzburg.de

*(T.B.) brixner@phys-chemie.uni-wuerzburg.de

Notes

The authors declare no competing financial interest

ACKNOWLEDGMENTS

We thank the DFG for funding this work within the Research Unit FOR 1809.

REFERENCES

(1) Brédas, J.-L.; Beljonne, D.; Coropceanu, V.; Cornil, J. *Chem. Rev.* **2004**, *104*, 4971.
(2) Scholes, G. D. *Annu. Rev. Phys. Chem.* **2003**, *54*, 57.
(3) Hwang, I.; Scholes, G. D. *Chem. Mater.* **2011**, *23*, 610.
(4) Hennebicq, E.; Pourtois, G.; Scholes, G. D.; Herz, L. M.; Russell, D. M.; Silva, C.; Setayesh, S.; Grimsdale, A. C.; Muellen, K.; Bredas, J.-L.; Beljonne, D. *J. Am. Chem. Soc.* **2005**, *127*, 4744.
(5) Beljonne, D.; Pourtois, G.; Silva, C.; Hennebicq, E.; Herz, L. M.; Friend, R. H.; Scholes, G. D.; Setayesh, S.; Mullen, K.; Bredas, J. L. *Proc. Natl. Acad. Sci. U. S. A.* **2002**, *99*, 10982.
(6) Becker, K.; Lupton, J. M. *J. Am. Chem. Soc.* **2006**, *128*, 6468.
(7) Banerji, N. *J. Mater. Chem. C* **2013**, *1*, 3052.
(8) Andrew, T. L.; Swager, T. M. In *Charge and Exciton Transport through Molecular Wires*; Siebbeles, L. D. A., Grozema, F. C., Eds.; Wiley-VCH Verlag GmbH & Co. KGaA: Weinheim, Germany, 2011.
(9) Laquai, F.; Park, Y.-S.; Kim, J.-J.; Basche, T. *Macromol. Rapid Commun.* **2009**, *30*, 1203.
(10) Gadermaier, C.; Lanzani, G. *J. Phys.: Condens. Matter* **2002**, *14*, 9785.
(11) Parkinson, P.; Muller, C.; Stingelin, N.; Johnston, M. B.; Herz, L. M. *J. Phys. Chem. Lett.* **2010**, *1*, 2788.

(12) Grage, M. M. L.; Pullerits, T.; Ruseckas, A.; Theander, M.; Inganas, O.; Sundstrom, V. *Chem. Phys. Lett.* **2001**, *339*, 96.

(13) Grage, M. M. L.; Wood, P. W.; Ruseckas, A.; Pullerits, T.; Mitchell, W.; Burn, P. L.; Samuel, I. D. W.; Sundstrom, V. *J. Chem. Phys.* **2003**, *118*, 7644.

(14) Dykstra, T. E.; Hennebicq, E.; Beljonne, D.; Gierschner, J.; Claudio, G.; Bittner, E. R.; Knoester, J.; Scholes, G. D. *J. Phys. Chem. B* **2009**, *113*, 656.

(15) Schwartz, B. J. *Nat. Mater.* **2008**, *7*, 427.

(16) Becker, K.; Fritzsche, M.; Hoeger, S.; Lupton, J. M. *J. Phys. Chem. B* **2008**, *112*, 4849.

(17) Talipov, M. R.; Boddeda, A.; Timerghazin, Q. K.; Rathore, R. *J. Phys. Chem. C* **2014**, *118*, 21400.

(18) Newbloom, G. M.; Hoffmann, S. M.; West, A. F.; Gile, M. C.; Sista, P.; Cheung, H.-K. C.; Luscombe, C. K.; Pfaendtner, J.; Pozzo, L. D. *Langmuir* **2015**, *31*, 458.

(19) Hoofman, R. J. O. M.; De Haas, M. P.; Siebbeles, L. D. A.; Warman, J. M. *Nature* **1998**, *392*, 54.

(20) Cho, S.; Rolczynski, B. S.; Xu, T.; Yu, L.; Chen, L. X. *J. Phys. Chem. B* **2015**, Ahead of Print.

(21) Ruseckas, A.; Wood, P.; Samuel, I. D. W.; Webster, G. R.; Mitchell, W. J.; Burn, P. L.; Sundstrom, V. *Phys. Rev. B: Condens. Matter Mater. Phys.* **2005**, *72*, 115214/1.

(22) Schwartz, B. J. *Annu. Rev. Phys. Chem.* **2003**, *54*, 141.

(23) Collini, E.; Scholes, G. D. *Science* **2009**, *323*, 369.

(24) Nguyen, T.-Q.; Wu, J.; Doan, V.; Schwartz, B. J.; Tolbert, S. H. *Science* **2000**, *288*, 652.

(25) Consani, C.; Koch, F.; Panzer, F.; Unger, T.; Köhler, A.; Brixner, T. **2005**, submitted.

(26) Unger, T.; Panzer, F.; Consani, C.; Koch, F.; Brixner, T. **2015**, submitted.

(27) Nguyen, T.-Q.; Doan, V.; Schwartz, B. J. *J. Chem. Phys.* **1999**, *110*, 4068.

(28) Yan, M.; Rothberg, L. J.; Kwock, E. W.; Miller, T. M. *Phys. Rev. Lett.* **1995**, *75*, 1992.

(29) Ruseckas, A.; Theander, M.; Valkunas, L.; Andersson, M. R.; Inganas, O.; Sundstrom, V. *J. Lumin.* **1998**, *76&77*, 474.

(30) Watanabe, A.; Kodaira, T.; Ito, O. *Chem. Phys. Lett.* **1997**, *273*, 227.

(31) Zhang, J. Z.; Kreger, M. A.; Hu, Q. S.; Vitharana, D.; Pu, L.; Brock, P. J.; Scott, J. C. *J. Chem. Phys.* **1997**, *106*, 3710.

(32) Völker, S. F.; Uemura, S.; Limpinsel, M.; Mingebach, M.; Deibel, C.; Dyakonov, V.; Lambert, C. *Macromol. Chem. Phys.* **2010**, *211*, 1098.

(33) Völker, S. F.; Schmiedel, A.; Holzapfel, M.; Renziehausen, K.; Engel, V.; Lambert, C. *J. Phys. Chem. C* **2014**, *118*, 17467.

(34) Völker, S. F.; Dellermann, T.; Ceymann, H.; Holzapfel, M.; Lambert, C. *J. Polym. Sci., Part A: Polym. Chem.* **2014**, *52*, 890.

(35) Völker, S. F.; Schmiedel, A.; Holzapfel, M.; Böhm, C.; Lambert, C. *Phys. Chem. Chem. Phys.* **2013**, *15*, 19831.

(36) Völker, S. F.; Lambert, C. *Chem. Mater.* **2012**, *24*, 2541.

(37) Jiang, J.-Q.; Sun, C.-L.; Shi, Z.-F.; Zhang, H.-L. *RSC Adv.* **2014**, *4*, 32987.

(38) Ajayaghosh, A. *Acc. Chem. Res.* **2005**, *38*, 449.

(39) Beverina, L.; Salice, P. *Eur. J. Org. Chem.* **2010**, 1207.

(40) Sreejith, S.; Carol, P.; Chithra, P.; Ajayaghosh, A. *J. Mater. Chem.* **2008**, *18*, 264.

(41) Yagi, S.; Nakazumi, H. *Top. Heterocycl. Chem.* **2008**, *14*, 133.

(42) Hu, L.; Yan, Z.; Xu, H. *RSC Adv.* **2013**, *3*, 7667.

(43) Beverina, L.; Sassi, M. *Synlett* **2014**, *25*, 477.

(44) Silvestri, F.; Irwin, M. D.; Beverina, L.; Facchetti, A.; Pagani, G. A.; Marks, T. J. *J. Am. Chem. Soc.* **2008**, *130*, 17640.

(45) Merritt, V. Y.; Hovel, H. J. *Appl. Phys. Lett.* **1976**, *29*, 414.

(46) Morel, D. L.; Ghosh, A. K.; Feng, T.; Stogryn, E. L.; Purwin, P. E.; Shaw, R. F.; Fishman, C. *Appl. Phys. Lett.* **1978**, *32*, 495.

(47) Wang, S.; Mayo, E. I.; Perez, M. D.; Griffe, L.; Wei, G.; Djurovich, P. I.; Forrest, S. R.; Thompson, M. E. *Appl. Phys. Lett.* **2009**, *94*, 233304.

(48) Mayerhöffer, U.; Deing, K.; Gruss, K.; Braunschweig, H.; Meerholz, K.; Würthner, F. *Angew. Chem. Int. Ed.* **2009**, *48*, 8776.

(49) Fan, B.; Maniglio, Y.; Simeunovic, M.; Kuster, S.; Geiger, T.; Hany, R.; Nuesch, F. *Int. J. Photoenergy* **2009**, 1.

(50) Wei, G.; Wang, S.; Renshaw, K.; Thompson, M. E.; Forrest, S. R. *ACS Nano* **2010**, *4*, 1927.

(51) Wei, G.; Lunt, R. R.; Sun, K.; Wang, S.; Thompson, M. E.; Forrest, S. R. *Nano Lett.* **2010**, *10*, 3555.

(52) Beverina, L.; Drees, M.; Facchetti, A.; Salamone, M.; Ruffo, R.; Pagani, G. A. *Eur. J. Org. Chem.* **2011**, *2011*, 5555.

(53) Wei, G.-D.; Xiao, X.; Wang, S.-Y.; Zimmerman, J. D.; Sun, K.; Diev, V. V.; Thompson, M. E.; Forrest, S. R. *Nano Lett.* **2011**, *11*, 4261.

(54) Wang, S.; Hall, L.; Diev, V. V.; Haiges, R.; Wei, G.; Xiao, X.; Djurovich, P. I.; Forrest, S. R.; Thompson, M. E. *Chem. Mater.* **2011**, *23*, 4789.

(55) Wei, G.; Xiao, X.; Wang, S.; Sun, K.; Bergemann, K. J.; Thompson, M. E.; Forrest, S. R. *ACS Nano* **2012**, *6*, 972.

(56) Chen, C.-H.; Cheng, W.-T.; Tsai, M.-L.; Huang, K.-T. *Ind. Eng. Chem. Res.* **2012**, *51*, 3630.

(57) Xiao, X.; Wei, G.; Wang, S.; Zimmerman, J. D.; Renshaw, C. K.; Thompson, M. E.; Forrest, S. R. *Adv. Mater.* **2012**, *24*, 1956.

(58) Deing, K. C.; Mayerhöffer, U.; Würthner, F.; Meerholz, K. *Phys. Chem. Chem. Phys.* **2012**, *14*, 8328.

(59) Kylberg, W.; Zhang, Y.; Aebersold, A.; Araujo de Castro, F.; Geiger, T.; Heier, J.; Kuster, S.; Ma, C.-Q.; Bauerle, P.; Nuesch, F.; Tisserant, J.-N.; Hany, R. *Org. Electron.* **2012**, *13*, 1204.

(60) Maeda, T.; Tsukamoto, T.; Seto, A.; Yagi, S.; Nakazumi, H. *Macromol. Chem. Phys.* **2012**, *213*, 2590.

(61) Bagnis, D.; Beverina, L.; Huang, H.; Silvestri, F.; Yao, Y.; Yan, H.; Pagani, G. A.; Marks, T. J.; Facchetti, A. *J. Am. Chem. Soc.* **2010**, *132*, 4074.

(62) Choi, H.; Kamat, P. V. *J. Phys. Chem. Lett.* **2013**, *4*, 3983.

(63) Maeda, T.; Arikawa, S.; Nakao, H.; Yagi, S.; Nakazumi, H. *New J. Chem.* **2013**, *37*, 701.

(64) Maeda, T.; Hamamura, Y.; Miyanaga, K.; Shima, N.; Yagi, S.; Nakazumi, H. *Org. Lett.* **2011**, *13*, 5994.

(65) Maeda, T.; Nakao, H.; Kito, H.; Ichinose, H.; Yagi, S.; Nakazumi, H. *Dyes Pigm.* **2011**, *90*, 275.

(66) Maeda, T.; Shima, N.; Tsukamoto, T.; Yagi, S.; Nakazumi, H. *Synth. Met.* **2011**, *161*, 2481.

(67) Ros-Lis, J. V.; Martinez-Manez, R.; Sancenon, F.; Soto, J.; Spieles, M.; Rurack, K. *Chem. Eur. J.* **2008**, *14*, 10101.

(68) Ros-Lis, J. V.; Martinez-Manez, R.; Soto, J. *Chem. Commun.* **2002**, 2248.

(69) Ajayaghosh, A.; Arunkumar, E.; Daub, J. *Angew. Chem. Int. Ed.* **2002**, *41*, 1766.

(70) Radaram, B.; Mako, T.; Levine, M. *Dalton Trans.* **2013**, *42*, 16276.

(71) Ananda Rao, B.; Kim, H.; Son, Y.-A. *Sens. Actuators, B* **2013**, *188*, 847.

(72) Volkova, K. D.; Kovalska, V. B.; Tatarets, A. L.; Patsenker, L. D.; Kryvorotenko, D. V.; Yarmoluk, S. M. *Dyes Pigm.* **2006**, *72*, 285.

(73) Tatarets, A. L.; Fedyunyayeva, I. A.; Dyubko, T. S.; Povrozin, Y. A.; Doroshenko, A. O.; Terpetschnig, E. A.; Patsenker, L. D. *Anal. Chim. Acta* **2006**, *570*, 214.

(74) Terpetschnig, E.; Szmacinski, H.; Ozinskas, A.; Lakowicz, J. R. *Anal. Biochem.* **1994**, *217*, 197.

(75) Thomas, J.; Sherman, D. B.; Amiss, T. J.; Andaluz, S. A.; Pitner, J. B. *Bioconjugate Chem.* **2007**, *18*, 1841.

(76) Renard, B.-L.; Aubert, Y.; Asseline, U. *Tetrahedron Lett.* **2009**, *50*, 1897.

(77) Gao, F.-P.; Lin, Y.-X.; Li, L.-L.; Liu, Y.; Mayerhöffer, U.; Spenst, P.; Su, J.-G.; Li, J.-Y.; Würthner, F.; Wang, H. *Biomaterials* **2014**, *35*, 1004.

(78) Arunkumar, E.; Fu, N.; Smith, B. D. *Chem. Eur. J.* **2006**, *12*, 4684.

(79) Gassensmith, J. J.; Arunkumar, E.; Barr, L.; Baumes, J. M.; DiVittorio, K. M.; Johnson, J. R.; Noll, B. C.; Smith, B. D. *J. Am. Chem. Soc.* **2007**, *129*, 15054.

(80) Xiang, Z.; Nesterov, E. E.; Skoch, J.; Lin, T.; Hyman, B. T.; Swager, T. M.; Bacskai, B. J.; Reeves, S. A. *J. Histochem. Cytochem.* **2005**, *53*, 1511.

(81) Müllen, K.; Wegner, G. *Electronic Materials: The Oligomer Approach*; Wiley-VCH: Weinheim, 1998.

(82) Cabanillas-Gonzalez, J.; Grancini, G.; Lanzani, G. *Adv. Mater.* **2011**, *23*, 5468.

(83) Mukamel, S. In *Oxford Series in Optical and Imaging Sciences*; Lapp, M., Nishizawa, J.-I., Snavely, B. J., Stark, H., Tam, A. C., Wilson, T., Eds.; Oxford University Press: New York, 1995; Vol. 6, p 209.

(84) Mukamel, S. *Annu. Rev. Phys. Chem.* **2000**, *51*, 691.

(85) Jonas, D. M. *Annu. Rev. Phys. Chem.* **2003**, *54*, 425.

(86) Cho, M. *Chem. Rev.* **2008**, *108*, 1331.

(87) Van Stokkum, I. H. M.; Larsen, D. S.; Van Grondelle, R. *Biochim. Biophys. Acta, Bioenerg.* **2004**, *1657*, 82.

(88) Snellenburg, J. J.; Laptenok, S. P.; Seger, R.; Mullen, K. M.; Stokkum, I. H. M. v. *J. Stat. Soft.* **2012**, *49*, 1.

(89) Mullen, K. M.; Stokkum, I. H. M. v. *J. Stat. Soft.* **2007**, *18*, 1.

(90) Snellenburg, J. J.; Dekker, J. P.; van Grondelle, R.; van Stokkum, I. H. M. *J. Phys. Chem. B* **2013**, *117*, 11363.

(91) Selig, U.; Langhojer, F.; Dimler, F.; Lohrig, T.; Schwarz, C.; Gieseking, B.; Brixner, T. *Opt. Lett.* **2008**, *33*, 2851.

(92) Humeniuk, A.; Mitric, R. **2015**, submitted.

(93) Yanai, T.; Tew, D. P.; Handy, N. C. *Chem. Phys. Lett.* **2004**, *393*, 51.

(94) Niehaus, T. A.; Suhai, S.; Della Sala, F.; Lugli, P.; Elstner, M.; Seifert, G.; Frauenheim, T. *Phys. Rev. B: Condens. Matter Mater. Phys.* **2001**, *63*, 085108/1.

(95) Elstner, M.; Porezag, D.; Jungnickel, G.; Elsner, J.; Haugk, M.; Frauenheim, T.; Suhai, S.; Seifert, G. *Phys. Rev. B: Condens. Matter Mater. Phys.* **1998**, *58*, 7260.

(96) Polyutov, S.; Kuehn, O.; Pullerits, T. *Chem. Phys.* **2012**, *394*, 21.

(97) Gaab, K. M.; Bardeen, C. J. *J. Phys. Chem. B* **2004**, *108*, 4619.